JACS
JOURNAL OF THE AMERICAN CHEMICAL SOCIETY

Article

pubs.acs.org/JACS

Exploring the Aldol Reaction using Catalytic Antibodies and "On Water" Organocatalysts from QM/MM Calculations

Kira Armacost and Orlando Acevedo*

Department of Chemistry, Biochemistry, Auburn University, Auburn, Alabama 36849, United States

Supporting Information

ABSTRACT: The aldol reaction between benzaldehyde and acetone has been investigated using QM/MM Monte Carlo calculations and free-energy perturbation theory to determine the origin of the enhanced rates and enantioselectivities (% ee) derived from an enamine-based catalytic antibody 33F12 and a chiral organocatalyst. Electrostatic stabilization of the general acid/base TyrL36 by TrpH103, SerH100, and AsnL34 enabled the 33F12 active site to exclusively adopt an *si*-face benzaldehyde orientation for C−C bond formation with the LysH93-enamine. Whereas preorganization was responsible for the exclusive (*S*)-aldol product in the antibody, the organocatalyst featuring a chiral diphenyl amino alcohol moiety instead derived its preferred (*R*)-aldol product from an interplay between sterics and electronic stabilization. The *si*-face benzaldehyde conformation had unfavorable interactions with the organocatalyst in contrast to the *re*-face. Gas-phase calculations predicted a 73% ee; however, solution boosted the % ee values despite similar reaction geometries. An "on water" environment, defined as a reaction that proceeds in an aqueous organic emulsion, yielded a computed 94% ee (exptl 93% ee) compared to a calculated 87% ee in "neat" acetone (exptl 85% ee). Specific hydrogen bonding between the interfacial waters and an amide oxygen on the catalyst was found to control the % ee. A more compact *si*-face transition structure reduced solvent accessibility to the amide oxygen with a "closed state" steric barrier compared to an "open state" for the *re*-face. New insight into the synthetically important aldol reaction and state-of-the-art methodology is presented herein.

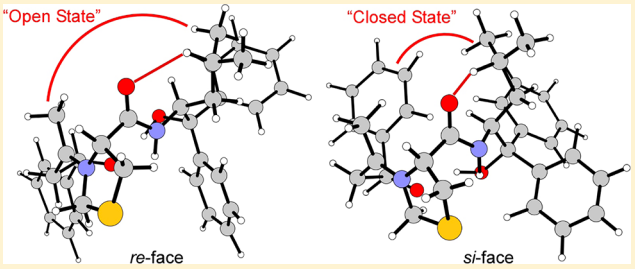

INTRODUCTION

The enantioselective aldol reaction is an important C−C bond formation reaction that has received considerable attention following the development of small proline-derived enamine-based catalysts by List, Barbas, and Lerner.[1,2] While the use of (*S*)-proline to catalyze asymmetric intramolecular aldol reactions began in the 1970s,[3] more recent derivatives of (*S*)-proline and (*S*)-prolinamide for the direct intermolecular aldol reaction between two carbonyl molecules have been developed that deliver high yields, 99:1 diastereoselectivies and enantioselectivities >99% ee.[4−9] Polar organic solvents have been widely used as a suitable solvent for the aldol reaction; however, many contemporary investigations have favored water as the reaction medium due to its low cost, ease of product isolation, and unique influence on the stereoselectivity of enamine-based organocatalytic aldol reactions.[10] Of particular interest are the recently reported aqueous-phase enantioselective catalysts by Singh and co-workers composed of a thiazolidine ring and a chiral diphenyl amino alcohol;[7,8] similar in structure to those first developed by Barbas[11] and Hayashi.[12] For example, the reaction between acetone and benzaldehyde using a Vishnumaya and Singh organocatalyst (Scheme 1) was reported to complete in 6 h in pure water compared to >16 h in acetone, and the subsequent product was obtained at 93% ee compared to 85% ee, respectively.[7]

Scheme 1. Aldol Reaction between Acetone and Benzaldehyde Using an Aqueous-Phase Organocatalyst or Catalytic Antibody 33F12

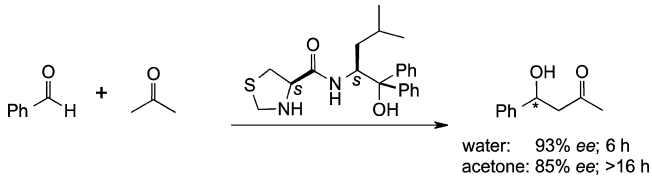

Singh and co-workers have proposed that the enamine-based aldol reaction proceeds via an "on water" environment that segregates the transition state away from the water molecules; this allows the reactants to benefit from the hydrophobic portion while stabilizing the amide oxygen via specific hydrogen bonding with the surface waters (Scheme 2).[7,8] "On water" conditions were first reported by Sharpless to give large rate increases and enhanced yields for a variety of reactions and is defined as a reaction that proceeds in an aqueous organic emulsion prepared by vigorously stirring insoluble reactants with water.[13] In contrast, reactants "in water" are dissolved homogeneously in water primarily through the use of cosolvents.[14] Superior yields and enantioselectivities for the

Received: June 5, 2013
Published: December 11, 2013

dx.doi.org/10.1021/ja405614p | J. Am. Chem. Soc. 2014, 136, 147−156

Scheme 2. Proposed Transition State for an "On Water" Enamine-Based Aldol Reaction

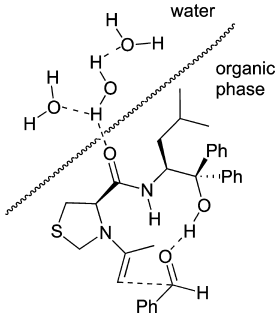

direct aldol of acyclic and cyclic ketones with different aldehydes in brine[7,8] relative to in water suggests an important 'salting out effect' indicative that water itself provides more than simply a medium for reaction.

Interestingly, catalysis of the aldol reaction via aldolase catalytic antibodies[15−18] laid the foundation for the asymmetric proline-based organocatalysts; however, mechanistic study of aldolase antibodies has proven to be more limited and difficult as compared to the organocatalysts.[5,19] A recently resolved crystal structure for catalytic antibody 33F12 with a 1,3-diketone has allowed direct observation of the enamine for the first time.[20] As enamines are generally unstable in water, both the antibody and on water reactions appear to rely in part on hydrophobicity to catalyze the reaction. For example, the pK_a of the ε-amino group of LysH93 (which reacts with acetone to form the enamine during reaction as shown in Scheme 3) has

Scheme 3. Aldol Reaction between Benzaldehyde, TyrL36, the Enamine Formed between Acetone and LysH93 in Catalytic Antibody 33F12

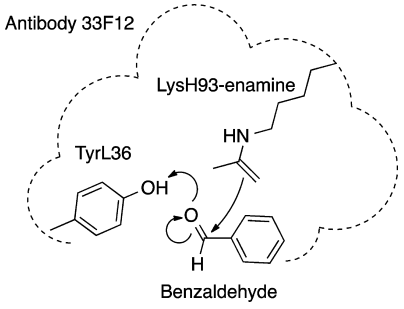

been estimated at 5.5 for antibody 33F12,[16] whereas the pK_a in free solution is 10.5.[18] In water, typical amines would be protonated and ineffective for reaction. A detailed atomic-level study upon the aldol reaction in both enzymatic and aqueous conditions would help elucidate the role of hydrophobic effects and specific hydrogen bonding upon the mechanism and enantioselectivities.

Mixed quantum and molecular mechanical (QM/MM) calculations coupled to free energy perturbation theory and Monte Carlo sampling (MC/FEP) were carried out here to clarify the enamine mechanism and the intermolecular interactions responsible for the amine catalysis and enhanced enantioselectivity using on water conditions and the aldolase antibody 33F12. The enamine mechanism with multiple organocatalysts has been investigated using density functional theory (DFT) methods by Houk and co-workers and provides a basis for comparison;[2,21−25] however, the origin behind the on water and antibody enhancements has not been examined. The reaction between acetone and benzaldehyde was simulated in this study with fully explicit environments using the aqueous organocatalyst shown in Scheme 1 and with antibody 33F12. The direct aldol reaction between acetone and benzaldehyde provides an immediate comparison between the diverse reaction conditions due to the availability of experimental data in both the aqueous and protein environments (Schemes 1 and 3).[16,20,26] Insight into the experimentally observed increase in enantioselectivity is given by computing the approach of the aldehyde from both the *re* and *si* faces. Additional calculations were performed in acetone to clarify the role of solvent. This work formulates a comprehensive theory on how both the aqueous surface boundary and the aldolase active site use sterics and specific hydrogen bonding to enhance rates and enantioselectivity for the aldol reaction.

COMPUTATIONAL METHODS

Setup and Processing for Antibody 33F12. Initial coordinates for the protein-based aldol system was obtained from a reported 1.9 Å crystal structure (PDB ID: 3FO9) of aldolase antibody 33F12 complexed with a 1,3-diketone hapten.[20] The raw PDB file was prepared for input to MCPRO through the chop program.[27] Chop outputs directives for the pepz program, which adds missing hydrogens, performs the residue truncation and capping, and converts the PDB file to a Z-matrix with OPLS atom typing that is suitable for input to MCPRO. Residues more than 15 Å from the binding site were removed for computational efficiency, which left one active site and 135 residues, including the light and heavy chains of the antibody nearest the ligand. The protein fragments furthest from the active site were made neutral, so no counterions were added. Benzaldehyde and the enamine formed between acetone and LysH93 were built and optimally positioned in the binding site by overlaying with the existing hapten ligand. The initial structure was relaxed via a conjugate gradient optimization to remove poor contacts.

QM/MM Method. All solutes and reacting antibody side-chains were treated using the PDDG/PM3 semiempirical QM method, which has given excellent results for a wide variety of organic and enzymatic reactions in the solution phase.[28−32] QM/MM calculations were run on a Linux cluster at Auburn University and on computers located at the Alabama Supercomputer Center. Protein simulations were carried out using the program MCPRO, while the condensed-phase reactions utilized BOSS.[27]

Condensed Phase. The on water reactions were carried out by removing the periodicity from the *z*-axis of an explicit 1235 water molecule box represented using the TIP4P water model,[33] and the solutes were placed on top of the *z*-axis; an equilibrated NVT water slab was used to prevent a very slow drift of the water molecules that reduces the exposed surface, i.e., stretch in the *z*-direction. Our method previously reproduced on water effects successfully for aromatic Claisen rearrangements.[30] A new OPLS-AA fully flexible solvent box for acetone was constructed in a fashion similar to previous work.[30] Briefly, the liquid-phase simulation was carried out by placing 400 acetone molecules at random positions within a periodic box. The system was then equilibrated at 25 °C for 225 million (M) MC steps in the NPT ensemble. A computed density of 0.798 g/cm^3 (exptl 0.7937 g/cm^3 at 293.15 K)[34] and heat of vaporization of 7.34 kcal/mol (exptl 7.47 kcal/mol)[35] compared favorably with experiment.

Periodic boundary conditions have been applied to the tetragonal boxes and solute−solvent, and solvent−solvent cutoffs of 12 Å were employed with quadratic feathering of the intermolecular interactions within 0.5 Å of the cutoff. Computation of the QM energy and atomic charges is performed for each attempted move of the solute, which occurs every 100 configurations. For electrostatic contributions to the solute−solvent energy, CM3 charges[36] were obtained for the solute with a scaling factor of 1.14. Lennard-Jones interactions between solutes and solvent atoms were taken into account using OPLS

dx.doi.org/10.1021/ja405614p | J. Am. Chem. Soc. 2014, 136, 147−156

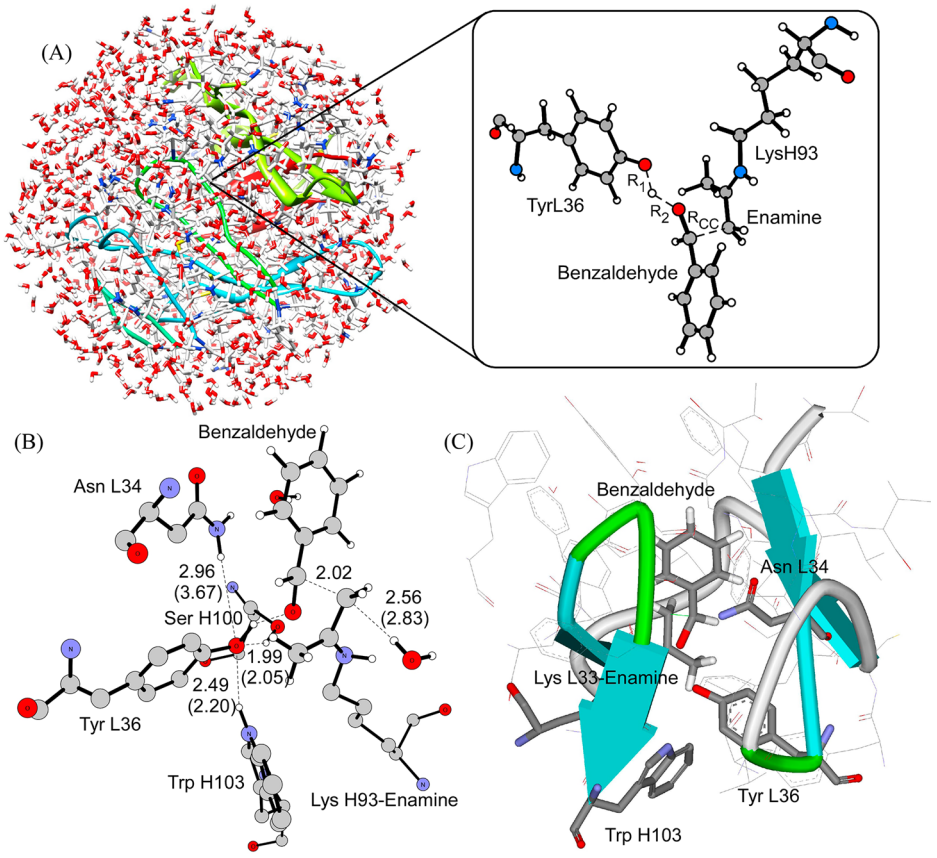

Figure 1. (A) Illustration of reduced antibody 33F12 consisting of 135 residues, benzaldehyde, TyrL36, the enamine formed between acetone and LysH93, and a 22 Å water cap. (B) A close-up of the transition-state region between the LysH93-enamine and benzaldehyde in the active site of antibody 33F12 with two nearby water molecules retained. Average distances given for transition structure (and ground state in parentheses) over the final 25 M configurations given in angstroms. (C) Benzaldehyde and LysH93-enamine shown in the binding pocket.

parameters. This combination is appropriate for a PM3-based method as it minimizes errors in the computed free energies of hydration.[37] Changes in free energy were calculated using free energy perturbation (FEP) theory in conjunction with NPT Metropolis Monte Carlo (MC) simulations at 25 °C and 1 atm. Each FEP window entailed ~40 M MC configurations of equilibration and 20 M configurations of averaging.

Aldolase Antibody 33F12. In our QM/MM implementation, benzaldehyde, the enamine formed between acetone and LysH93, and TyrL36 were treated with the PDDG/PM3 semiempirical QM method. The remainder of the protein utilized the OPLS-AA force field.[38] The interactions of overlapped atoms in the QM and MM regions are described through "link atoms" using hydrogens in the QM calculation.[39] The connection of the QM and MM regions requires the inclusion of the classical bond stretching, angle bending, and torsion terms if any MM atom is involved in the interaction. CM3 charges were obtained for the QM active site with a scaling factor of 1.12. At the beginning of the MC simulations, a water cap with 22 Å radius (~900 TIP4P waters) was added. A half-harmonic potential with a force constant of 1.5 kcal mol^{-1} $Å^{-2}$ was applied to water molecules at a distance >22 Å. To ensure that the final orientation of the water molecules within the aldolase binding pocket was not an artifact of the water cap, multiple reaction pathway simulations with different caps were carried out.

MC Simulation Protocol. All simulations were run at 25 °C using MC statistical mechanics. Adjustments to the allowed ranges for rotations, translations, and dihedral angle movements for the solution-based calculations led to overall MC acceptance rates of 30−50% for new configurations. The ranges for bond stretching and angle bending were set automatically by the BOSS program on the basis of force constants and temperature. For the antibody, only the bond angles and dihedrals of side chains of residues with any atom within 10 Å of the center of the system are varied. All degrees of freedom in the QM region are varied, except the carbon atom adjacent to the link atom and those involved in the reaction coordinates. Each simulation for a FEP window consists of 5 M configurations of solvent relaxation, where the water molecules were moved randomly while keeping the protein and substrate fixed, followed by 10 M configurations of full equilibration, where all degrees of freedom are varied, and 25 M configurations of averaging, where all degrees of freedom were sampled and the free-energy changes were obtained. Stability in the computed energies, free energies, and volume (for NPT) were used to monitor convergence of the MC simulations. During the simulations, 10% of the attempted MC moves involve the active site and 1% the QM region. Each move of the QM region requires one self-consistent field QM calculation if the move is rejected and three if accepted (reference and two perturbed structures). Therefore, each protein FEP window requires ~0.5−1 million QM calculations; the total for this work exceeded 500 M configurations.

Polynomial Quadrature Method. In our recent work elucidating the mechanism for fatty acid amide hydrolase (FAAH) and antibody 4B2, significant technical advances were reported for the treatment of proton-transfer reactions.[32,39] For a typical proton transfer, O−H···O′ → O···H−O′, it was found that the O···O′ distance remains relatively constant and that r(O−H) − r(H−O′) can be used to compute a 1-D potentials of mean force (PMF). This normally requires approximately 30 to 50 double-wide FEP windows using 0.02 Å Δr increments, while ~900 windows would be needed for a 2-D PMF using two distances as reaction coordinates. However, free-energy changes for individual windows can be fit almost perfectly by a fifth order polynomial. Analytical integration yields a sextic polynomial for the overall proton-transfer PMF. This allows for the accurate construction of the full

dx.doi.org/10.1021/ja405614p | J. Am. Chem. Soc. 2014, 136, 147−156

Scheme 4. Proposed Enamine Mechanism for Aldol Reaction in Antibody 33F12 (ref [20])[a]

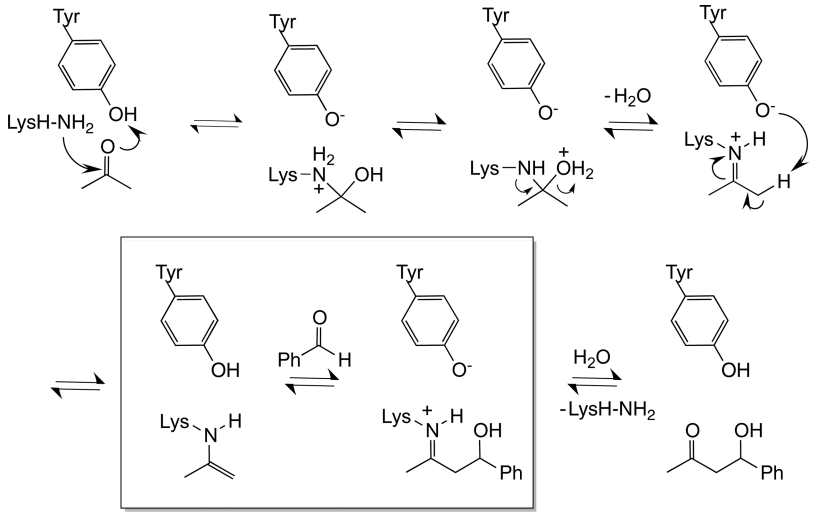

[a]The current calculations are emphasized within the box.

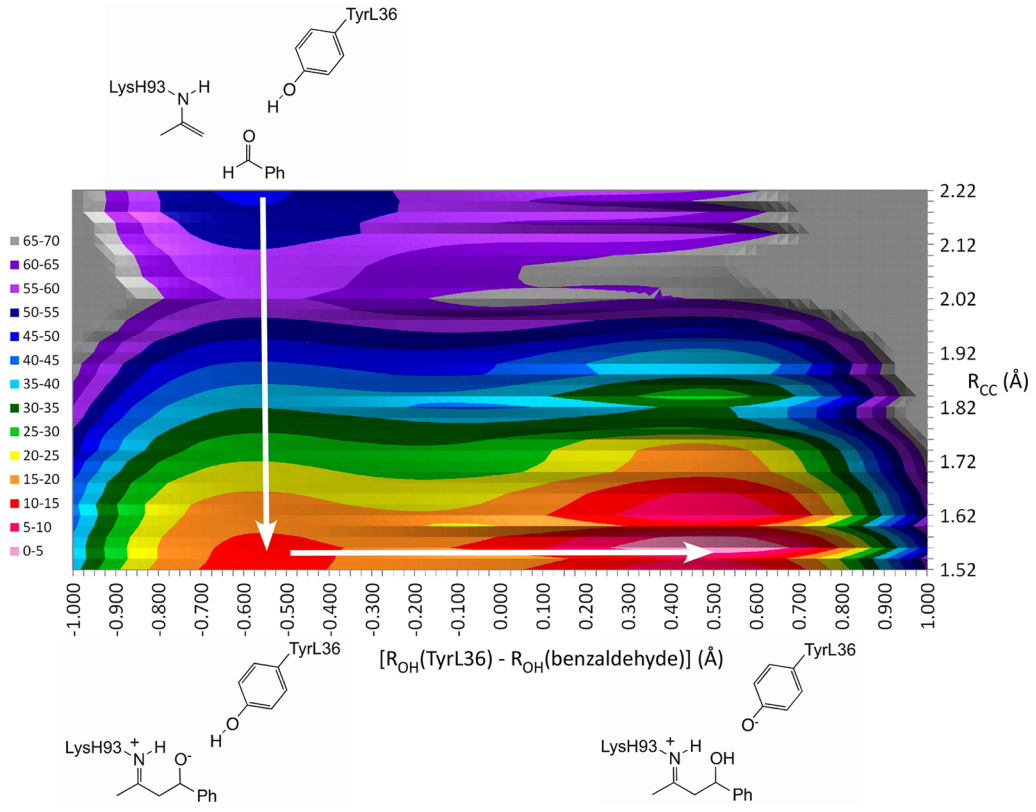

Figure 2. Free-energy profile (kcal/mol) for the aldol reaction between benzaldehyde, the enamine formed between acetone and LysH93, and TyrL36 in antibody 33F12. [R_{OH}(TyrL36) + R_{OH}(benzaldehyde)] fixed at 2.6 Å. Maximum free-energy values are truncated to 70 kcal/mol for clarity.

PMF using only 7 FEP windows instead of the usual 50.[29,32,40] The largest deviation found between the approximate and the detailed calculation was 0.5 kcal/mol.

RESULTS AND DISCUSSION

Aldol Reaction in Antibody 33F12. PMF calculations were used to build a free energy map, ΔG (kcal/mol), for the aldol reaction in antibody 33F12 using the reaction coordinates between the LysH93-enamine and benzaldehyde C−C bond (R_{CC}) and the proton transfer, $R_1 - R_2$, between the TyrL36 and benzaldehyde oxygen atoms (see Figure 1). A fixed distance of $R_1 + R_2 = 2.6$ Å was established to be appropriate from test simulations and prior work.[39] Kinetic experiments on pH-rate profiles and enolization catalysis for aldolase antibody 78H6 suggest that the C−C bond formation step highlighted in Scheme 4 should be both rate and enantioselectivity determining.[41] Additional study of aldol antibodies 33F12 and 38C2, which afford the (*S*)-aldol product, along with 84G3

dx.doi.org/10.1021/ja405614p | J. Am. Chem. Soc. 2014, 136, 147−156

and 93F3, that yield the (*R*)-aldol product, provided further evidence of the enantioselectivity being dictated by the C−C bond forming step.[15,16,18,26,42] In addition, TyrL36 is believed to function as a general acid and base in antibody 33F12 as shown in the projected mechanism (Scheme 4).[20] The role of TyrL36 has been supported by the TyrL36Phe mutant of aldolase antibody 38C2, which does not bind to the diketones, but yields an (*S*)-aldol product between a ketone and an aromatic aldehyde similar to 33F12.[20]

The enzymatic reaction was predicted to follow a stepwise mechanism where the enamine benzaldehyde C−C distance began at a separation of 2.22 Å as larger distances became energetically unfavorable due to poor steric interactions within the active site pocket. The R_{CC} bond distance at the transition state was calculated to be 2.02 Å (Figure 1B) and proceeded to a geometry of 1.54 Å for the intermediate where the C−C bond is fully developed, but the proton transfer had not occurred (Figure 2). A $\Delta G^{\ddagger}$ of 10.2 ± 1 kcal/mol was computed for the bond formation, and the subsequent proton transfer between the TyrL36 and benzaldehyde oxygens occurred rapidly with a $\Delta\Delta G^{\ddagger}$ of 2.1 kcal/mol. The energetics are consistent with a previously computed MP2/6-31G(d,p) value of 10.1 kcal/mol for the "theozyme" aldol reaction between a primary enamine and acetaldehyde using an implicit PCM solvent model (a permittivity value of ε = 10.4 was used for similarity to the *n*-octanol medium believed to resemble the active site of 33F12).[43] The MP2 optimized transition-state R_{CC} distance of 1.944 Å was also reasonable compared to the current geometry value of 2.02 Å. DFT-based calculations resulted in similar energies and geometries.[21]

While the QM/MM and MP2/PCM methods predicted identical activation barriers for the enzymatic aldol reaction, both values are likely underestimated compared to experiment. In addition, the computed ΔG_{rxn} of −49.2 kcal/mol between the enamine reactants and the iminium cation intermediate is almost certainly overestimated. Deviation from experimental values can often be attributed to systematic errors in computed energies when employing semiempirical methods in the QM/MM methodology.[28] For example, PDDG/PM3/MM calculations were used to study the ring-opening of 5-nitrobenzisoxazole in Baker's *de novo* designed Kemp elimination enzymes.[44] The predicted activation barriers were considerably underestimated compared to experiment, e.g., 8.1 ± 1 kcal/mol (exptl 20.0 kcal/mol) for KE07 and 12.3 ± 1 kcal/mol (exptl 19.8 kcal/mol) for KE15. These results could be taken as an indication of a poorly represented microenvironment, however those calculations qualitatively predicted with high accuracy which enzymes would be catalytically active and were an essential part of the design process. Relative energy values between enzymatic mutants or different solvents may predict close agreement with experiment (shown for the organocatalyst later); however, improving absolute barriers will require more advanced QM methods. Work is currently underway to incorporate DFT and ab initio methods into the current software,[27] but compromises in system size or sampling may result as a consequence.

A strong hydrogen-bond network featuring TrpH103 and hydrophilic residues SerH100 and AsnL34 helped anchor the TyrL36 residue in an appropriate position to participate in a proton transfer and adopt the correct enantioselective *si*-face orientation for benzaldehyde with the LysH93-enamine (Figure 1C). Inspection of the active site finds the *re*-face of benzaldehyde would incur poor steric interactions with TyrL36 and its supporting residues. Docking simulations of reduced DFT-based transition structures of methylamine in place of the ε-amino group into the 33F12 active site also supported a geometric origin for the enantiopreference of (*S*)-aldol products.[26] From the current simulations, TrpH103 points its hydrogen atom at the oxygen of TyrL36 at an average distance of 2.20 and 2.49 Å at the ground and transition states of the reaction pathway, respectively (Figure 1B). The SerH100 forms tighter hydrogen bonds with the TyrL36 oxygen at distances of 2.05 and 1.99 Å, for the reactants and transition states, respectively, while AsnL34 provides longer hydrogen-bond distances of 3.67 and 2.96 Å (Figure 1B).

The reactive LysH93 residue in catalytic antibody 33F12 is surrounded primarily by hydrophobic residues resulting in a microenvironment that has been suggested to approximate that of *n*-octanol.[16] However, following the C−C bond formation and proton transfer, interaction with water is crucial for the hydrolysis of the iminium cation intermediate toward the final aldol adduct (Scheme 4). In general, the implications of water-mediated active sites are broad, as a study of theoretically designed and experimentally tested retro-aldol enzymes found that the explicit inclusion of water molecules into the active site gave significant rate enhancements of up to 4 orders of magnitude greater than those that simply relied on charged side-chain networks.[45] In addition, our computational study of catalytic antibody 4B2 found the role of water to be essential in the catalysis of the mechanistically different Kemp elimination and allylic rearrangement reactions.[32]

A snapshot taken at the end of the MC simulations near the transition-state region found up to 6 water molecules within 5.0 Å of the benzaldehyde (Figure S1). One water molecule was located near the enamine throughout the reaction forming an average interaction distance of 2.20 Å with the nitrogen at the reactants and a longer value of 2.61 Å at the transition state. The lone water, located in a hydrophobic portion of the active site, interacted primarily with the active site residue SerH35 and maintained a distance of 1.8−1.9 Å with the Ser oxygen at the transition state. As a point of reference, the same water molecule was adjacent to the terminal reacting sp^2 carbon on the LysH93-enamine with longer distances of 2.83 and 2.56 Å at the ground and transition states, respectively (Figure 1B). An additional water molecule was found to hydrogen bond with the π-system of the aromatic benzaldehyde ring (Figure 1B). There were no waters interacting directly with TyrL36 throughout the C−C bond forming process. Site-specific electrostatic stabilization of the TyrL36 phenoxide was provided exclusively by the adjacent hydrophilic residues. Water may play a larger role during the other portions of the mechanism, e.g., hydrolysis of the iminium.

Aldol Reaction with an Organocatalyst in Solution. Free energies of activation were also computed for the aldol reaction between acetone and benzaldehyde catalyzed by the organocatalyst[7] from Scheme 1 in acetone and on water (Figure 3). The enamine-based aldol reaction was carried out from both the *re*- and *si*-faces of benzaldehyde. Gas-phase PDDG/PM3 optimized transition structures using the Gaussian 09 software[46] found the same mechanism as the catalytic antibody with a single imaginary frequency used to verify the C−C bond formation and proton-transfer transition states. Solution-phase QM/MM calculations were carried out in a similar fashion to the 33F12 simulations, where the enamine-benzaldehyde C−C bond (R_{CC}) was perturbed in increments of 0.01 Å to a final 3.10 Å separation. The energy became flat in this separation

dx.doi.org/10.1021/ja405614p | J. Am. Chem. Soc. 2014, 136, 147−156

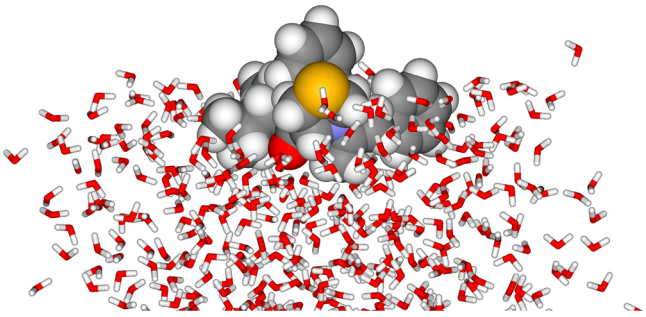

Figure 3. Illustration of the on water organocatalyst-enamine *re*-face benzaldehyde transition structure from the QM/MM simulations.

region and remained flat up to 4 Å, as tested for the on water *re*-face simulation. The R_{CC} bond formation energy was exclusively computed in solution due to the large computational resources required. The calculated transition-state reacting distances on water and in acetone are given in Table 1 with an estimated error of ±0.02 Å. As a point of comparison,

Table 1. Calculated R_{CC} Bond Lengths (Å) for the Aldol Reaction Transition Structure between the Organocatalyst-Enamine and Benzaldehyde[a]

	on water	acetone	gas
re-face	1.80	1.74	1.69
si-face	1.82	1.76	1.68

[a]QM/MM MC/FEP.

gas-phase ab initio R_{CC} bond distances for related aldol reactions are generally in the 1.9 Å range.[9] The geometries predicted the reaction to yield a later transition state in acetone with a R_{CC} around 1.74−1.76 Å compared to 1.80−1.82 Å on water, which is consistent with a more compact transition state in the "neat" solution. Gas-phase calculations found R_{CC} transition-state distances shorter than in acetone (Table 1). Enhanced electrostatic stabilization of the emerging charges on the transition states is linked to an increasing solvent polarity. Specific interactions between water and acetone with the substrates are discussed in detail later (solute−solvent energy pair distributions and radial distribution functions).

The reaction in acetone gave $\Delta G^{\ddagger}$ barriers of 29.6 and 31.2 kcal/mol for the *re*- and *si*-faces of benzaldehyde, respectively, while the on water environment yielded 26.9 and 29.0 kcal/mol (Table 2). It should be noted that enantioselectivity is controlled during C−C bond formation,[22] but the rate may be dictated by a separate step in the enamine mechanism. For example, ^{13}C kinetic isotope effect experiments by Meyer and collaborators have determined the rate-limiting step to precede enamine formation in a proline-catalyzed intramolecular aldol reaction.[24] Uncertainties in the free energy barriers were determined by propagating standard deviations (σ_i) of only 0.01−0.02 kcal/mol on each individual ΔG_i. Smooth free energy profiles were obtained with overall $\Delta G^{\ddagger}$ uncertainties of ±0.2 kcal/mol. The $\Delta\Delta G^{\ddagger}$ and enantioselectivity (% ee) values for the solution and gas-phase aldol reactions are given in Table 3.

Table 2. Calculated Free Energies of Activation, $\Delta G^{\ddagger}$ (kcal/mol), at 25 °C for the Aldol Reaction Between the Organocatalyst-Enamine and the *re*- and *si*-Faces of Benzaldehyde[a]

solvent	$\Delta G^{\ddagger}$ (*re*)	$\Delta G^{\ddagger}$ (*si*)
on water	26.9	29.0
acetone	29.6	31.2

[a]QM/MM MC/FEP.

Table 3. Free Energy of Activation Difference, $\Delta\Delta G^{\ddagger}$ (kcal/mol), and Enantioselectivity, % ee, at 25 °C for the Aldol Reaction Between the Organocatalyst-Enamine and the *re*- and *si*-Faces of Benzaldehyde

solvent	$\Delta\Delta G^{\ddagger}$ (calcd)	% ee (calcd)	% ee (exptl)[a]
on water	2.1	94	93[b], 95[c]
acetone	1.6	87	85
gas	1.1	73	–

[a]Ref 7; 5 mol % catalyst, rt. [b]Water. [c]Brine.

In addition to the close % ee agreement with experiment, the predicted absolute $\Delta G^{\ddagger}$ values also agreed well with recent gas-phase DFT studies. For example, Houk and co-workers computed the aldol reaction between acetone and benzaldehyde using an organocatalyst containing the thiazolidine ring, but a carboxylic group in place of the chiral amino alcohol shown in Scheme 1. Their B3LYP/6-31G(d,p) calculated *re*- and *si*-face enthalpies of activation were 25.5 and 26.7 kcal/mol with respect to the separated reactants;[25] the gas-phase $\Delta\Delta H^{\ddagger}$ of 1.2 kcal/mol also matched well with PDDG/PM3 (Table 3). In general, all the proline derivatives and 2-azetidine carboxylic acid catalysts yielded activation enthalpies of 20−27 kcal/mol,[25] which is consistent with the range of energies predicted in the current study using the QM/MM methodology.

The on water environment reduced the $\Delta G^{\ddagger}$ compared to acetone by 2.7 and 2.2 kcal/mol for the *re*- and *si*-face benzaldehyde aldol reactions, respectively. Water played a crucial role by increasing the % ee of the aldol reaction, where Singh reported increased equivalents of water improved enantioselectivity from 87% to 97%.[7] Figure 4 gives representative on water QM/MM transition structures for the organocatalyst-enamine reacting with the *re*- and *si*-faces of benzaldehyde. It is immediately clear that the *si*-face orientation has the potential for poorer steric interactions compared to the *re*-face. For example, a hydrogen atom on the *si*-face benzaldehyde ring is 1.53 Å from the hydrogen atom attached to the α-carbon adjacent to the amide nitrogen; a second hydrogen on the ring is 1.81 Å from a hydrogen atom located on the isobutyl group (Figure 4). However, gas-phase PDDG/PM3 optimizations accounted for only a 73% ee compared to 94% on water (Table 3). As the aqueous and vacuum transition structure conformations were similar, both systems should experience similar steric effects. Therefore, the boosted % ee in solution is likely due to an enhanced electronic stabilization.

An orientation analysis of the aldol transition states relative to the surface of the slab of 1235 waters found hydrogen bonding between the interfacial waters and the amide oxygen as predicted in Scheme 2; however, the current simulations determined that the benzaldehyde and carbonyl oxygen atoms responsible for the subsequent proton transfer were also immersed in water (Figure 3). In addition, the benzaldehyde ring benefited from favorable interactions between water and the π-system of the aromatic ring, similar to the active site of antibody 33F12. The organocatalyst-enamine phenyl rings and the isobutyl substituents were observed to reside primarily in

dx.doi.org/10.1021/ja405614p | J. Am. Chem. Soc. 2014, 136, 147−156

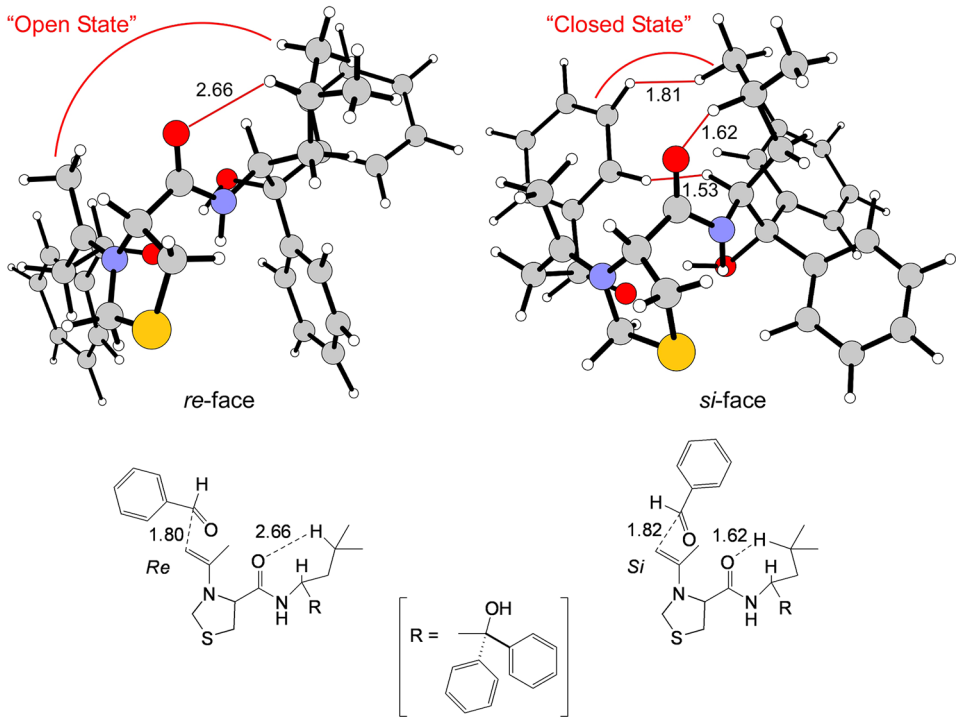

Figure 4. Organocatalyst-enamine transition states from the on water simulations with the *re*- and *si*-face benzaldehyde conformations. The "open state" represents a greater solvent accessible surface area for the amide oxygen compared to the "closed state".

vacuum (or the "organic phase") throughout the entire simulation. The partially solvated structure (Figure 3) correlates well with the superior yields, and enantioselectivities reported in brine as the 'salting out effect' increased the 'hydrophobic effect'.[4]

To investigate the origin behind the enhanced enantioselectivity reported on water, solute−solvent energy pair distributions were computed for FEP windows near the transition structures (Figure 5). Solute−solvent energy pair

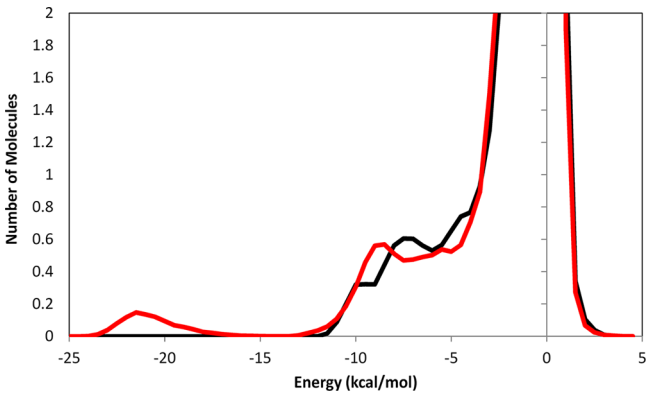

Figure 5. Solute−solvent energy pair distributions for the on water aldol reaction between the organocatalyst-enamine and the *re*- and *si*-face (red and black, respectively) benzaldehyde transition structures at 25 °C.

distributions note the average number of water molecules that interact with the aldol reaction. Highly favorable hydrogen-bonding interactions between the solute and solvent components are reflected in the left-most region with energies more attractive than approximately −5 kcal/mol. A large band centered at 0 kcal/mol arises from the many molecules located in the outer solvation shells. Intriguingly, the on water *re*-face transition structure benefited dramatically from the aqueous environment as a peak developed with an average strength of −22 kcal/mol that was not observed in the *si*-face transition state. The calculations suggest a greater accessibility of water to the oxygen atoms in the *re*-face orientation compared to the *si*-face, possibly a consequence of improved sterics between the organocatalyst-enamine and benzaldehyde. NMR studies have emphasized conformational preferences of enamines, e.g., prolinol, linked to specific stereoselective outcomes.[47]

Integration of the energy bands from −25 to −4 kcal/mol (or −3.5 kcal/mol) resulted in ∼1 additional water molecule interacting with the *re*-face transition state as compared to the *si*-face orientation (Table 4). Conversely, integration of the

Table 4. Solute−Solvent Energy Pair Distributions for the Organocatalyst-Enamine and Benzaldehyde Transition Structures On Water Integrated to −4.0 kcal/mol[a]

	re-face	*si*-face
on water	8.1 (9.0)	7.3 (8.2)
acetone	7.1 (8.7)	7.1 (8.9)

[a]From Figures 5 and S2; −3.5 kcal/mol in parentheses.

solute−solvent energy bands for the reaction in acetone (Figure S2) finds essentially no difference between the number of solvent molecules interacting with the *re*- and *si*-face transition structures. Acetone's weaker and less specific dipole−dipole interactions between the solvent and the transition structures led to diminished interactions correlated to increased activation barriers.

The solute−solvent interactions for the aldol reaction on water can be further characterized by radial distribution functions, $g(R)$. Hydrogen bonding between the amide oxygen, O(amide), the alcohol oxygen, O(alcohol), or the benzalde-

dx.doi.org/10.1021/ja405614p | J. Am. Chem. Soc. 2014, 136, 147−156

hyde oxygen, O(benz), and a hydrogen atom on water, H(water), should yield contacts shorter than 2.7 Å. Accordingly, the on water reactions show well-defined first peaks centered around 1.7−1.8 Å with a minimum around 2.5−2.6 Å that reflects the hydrogen bonds (Figure 6). The

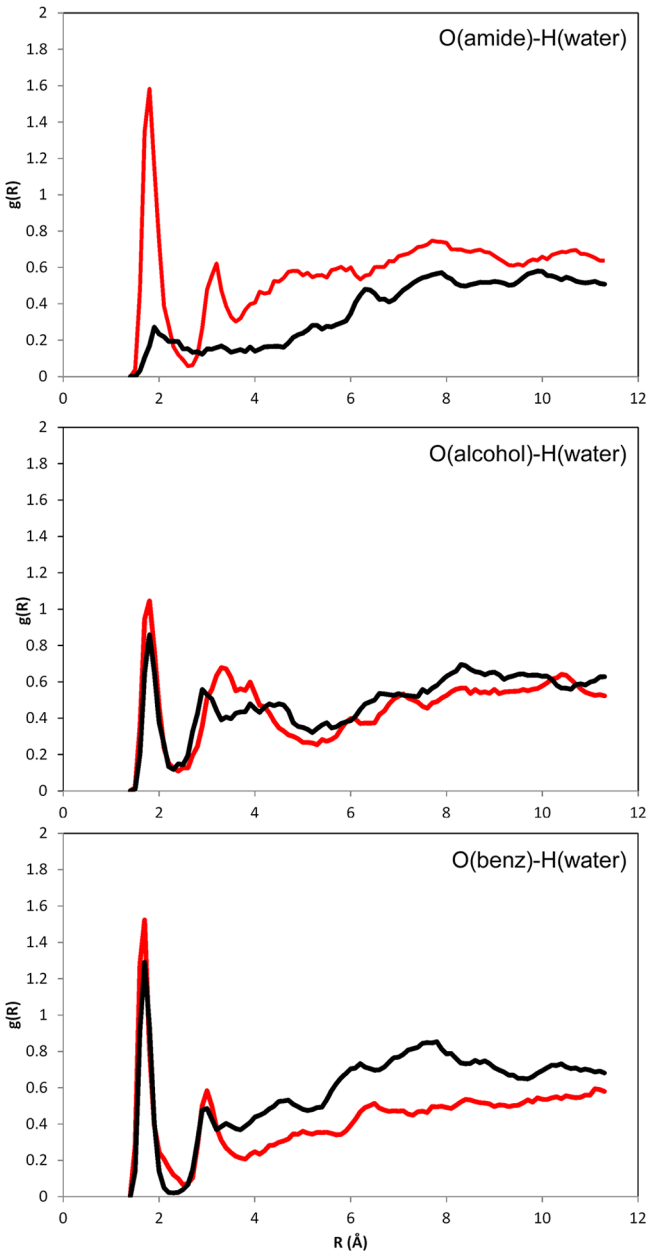

Figure 6. Computed O(amide), O(alcohol), and O(benzaldehyde) atoms and H(water) radial distribution functions for the on water *re*- and *si*-face (red and black, respectively) aldol reaction transition structures at 25 °C.

O(alcohol)−H(water) and O(benz)−H(water) display similar interaction peak heights with the interfacial waters for both the *re*- and *si*-face transition structures. Integration of these peaks for water interacting with the alcohol and benzaldehyde oxygens finds a slight increase for the *re*-face with 1.3 and 1.4 waters, respectively, compared to 1.0 water at each interaction site for the *si*-face orientation (Table 5).

The interaction of water with the amide oxygen differs considerably between the transition structure conformations. In

Table 5. Number of Water Molecules Interacting with the Oxygen Atoms from the Organocatalyst-Enamine, O(amide) and O(carbonyl) and with the Oxygen Atom on Benzaldehyde, O(benz), for the Aldol Transition Structures

	re-face	*si*-face
O(amide)	2.0	1.0
O(carbonyl)	1.3	1.0
O(benz)	1.4	1.0

[a]Integration of the first peak of Figure 6.

the case of the *re*-face reaction, the large peak demonstrates considerable O(amide)−H(water) hydrogen bonding, whereas the *si*-face exhibits a significantly smaller interaction peak (Figure 6). Integration of these peaks from 0 to 2.5−2.7 Å finds an additional site-specific O(amide)−H(water) hydrogen bond for the *re*-face transition structure (Table 5). The computed atomic CM3 charges on the amide oxygen are similar, i.e., −0.54 versus −0.50 e, for the *re*- and *si*-face transition structures. Thus, an enhanced electrostatic interaction at the *re*-face transition structure is not the origin of the additional complexing water. Instead, the more compact *si*-face transition structure reduces the solvent accessibility with a "closed state" steric barrier between the isobutyl group and the amide oxygen of 1.62 Å (Figure 4). The energetically favored *re*-face transition structure has an "open state" with an increased distance of 2.66 Å between the atoms. Accordingly, the computed solvent accessible surface area (SASA) for the *re*-face transition structure was 827 Å^2 and the *si*-face was 762 Å^2. The results are consistent with our previous work showing that unique positioning of a *tert*-butyl C_2-substituent in a bis(oxazoline)-Cu(II) catalyzed Diels−Alder reaction controlled *endo* selectivity.[48]

CONCLUSIONS

In summary, QM/MM and MC/FEP calculations have been performed for the aldol reaction between benzaldehyde and acetone catalyzed by catalytic antibody 33F12 and a Vishnumaya and Singh organocatalyst containing a thiazolidine ring and a chiral diphenyl amino alcohol moiety (Scheme 1). Excellent agreement between computed and experimental enantioselectivities (% ee) and free energies of activation were reported. The aldol reaction was predicted to follow a stepwise enamine mechanism that reproduced kinetic experiments and found the C−C bond formation step to be enantioselectivity determining.[41] A calculated $\Delta G^{\ddagger}$ of 10.2 ± 1 kcal/mol was predicted for the bond formation in antibody 33F12, and the subsequent proton transfer between the TyrL36 and benzaldehyde oxygens occurred rapidly with a $\Delta\Delta G^{\ddagger}$ of 2.1 kcal/mol. A strong hydrogen-bond network featuring TrpH103 and hydrophilic residues SerH100 and AsnL34 helped anchor the TyrL36 residue in an appropriate position to participate in a proton transfer and adopt the correct enantioselective *si*-face orientation for benzaldehyde with the LysH93-enamine (Figure 1). Inspection of the active site found a geometric origin for the enantiopreference of (*S*)-aldol products, as the *re*-face of benzaldehyde would incur poor steric interactions with TyrL36 and its supporting residues. No water molecules were found to directly interact with TyrL36 throughout the C−C bond forming process. However, one water molecule was located near the enamine that primarily interacted with active site residue SerH35 throughout the reaction. An additional water molecule was found to hydrogen bond with the π-system of the

dx.doi.org/10.1021/ja405614p | J. Am. Chem. Soc. 2014, 136, 147−156

aromatic benzaldehyde ring. Overall, water did not participate directly with the reaction but may play a larger role during the other portions of the mechanism, e.g., hydrolysis of the iminium.

Conversely, the organocatalyst-based aldol reaction in solution relied directly on water to enhance the % ee. Singh and co-workers have proposed that the enamine-based aldol reaction proceeds via an "on water" environment that segregates the transition state away from the water molecules; this allows the reactants to benefit from the hydrophobic portion while stabilizing the amide oxygen via specific hydrogen bonding with the surface waters (Scheme 2).[7,8] Solution-phase calculations were performed using explicit solvent to reproduce both the on water and acetone environments. The reaction in acetone gave $\Delta G^{\ddagger}$ barriers of 29.6 and 31.2 kcal/mol for the *re*- and *si*-faces of benzaldehyde, respectively, while the on water environment yielded 26.9 and 29.0 kcal/mol. The % ee was enhanced with increasing solvent polarity, e.g., computed 87% and 94% ee in acetone and on water, respectively (exptl = 85% and 93%). The *si*-face orientation has the potential for poorer steric interactions compared to the *re*-face. However, gas-phase calculations predicted a 73% ee despite similar geometries to the solution-phase structures. The observations suggest that the % ee enhancement from the solvent is derived from enhanced electrostatic stabilization.

To investigate the origin behind the superior enantioselectivity reported on water, solute−solvent energy pair distributions and radial distribution functions were computed for FEP windows near the transition structures. Integration of the solute−solvent energy bands for the reaction on water finds an additional water molecule complexing to the *re*-face transition structure compared to the *si*-face. Integration of the radial distribution functions finds the extra water interacts with the amide oxygen of the *re*-face conformation. Calculations of the atomic CM3 charges on the amide oxygen ruled out an enhanced electrostatic interaction at the *re*-face transition structure as the origin of the boosted % ee. Instead, a more compact *si*-face transition structure reduced the solvent accessibility with a "closed state" steric barrier between the isobutyl group and the amide oxygen. The energetically favored *re*-face transition structure has an "open state" with an increased distance of between the atoms.

Overall, the simulations predicted that addition of substituents to aqueous organocatalysts that reduce solvent accessibility exclusively to the *si*-face attack should improve % ee for the asymmetric aldol reaction. Going forward with this knowledge, a chemist may wish to synthesize variants that show even greater differences in the SASA between the *re*- and *si*-face transition states (a simple gas-phase QM calculation could provide proper suggestions for substituents as the reacting geometries were generally found to be within 0.1 Å of the solution-phase structures).

■ ASSOCIATED CONTENT

Supporting Information

Energies, frequencies, and coordinates of all gas-phase structures computed using the PDDG/PM3 method; additional figure of the aldolase active site; solute−solvent energy pair distributions in acetone; and complete ref 46. This material is available free of charge via the Internet at http://pubs.acs.org.

■ AUTHOR INFORMATION

Corresponding Author

orlando.acevedo@auburn.edu

Notes

The authors declare no competing financial interest.

■ ACKNOWLEDGMENTS

Gratitude is expressed to the National Science Foundation (CHE-1149604) and the Alabama Supercomputer Center for support of this research and to Dr. Billy McCann for assistance. Suggestions given from an anonymous reviewer that improved the manuscript are also appreciated.

■ REFERENCES

(1) (a) List, B.; Lerner, R. A.; Barbas, C. F., III *J. Am. Chem. Soc.* **2000**, *122*, 2395−2396. (b) List, B. *Tetrahedron* **2002**, *58*, 5573−5590. (c) Notz, W.; Tanaka, F.; Barbas, C. F., III *Acc. Chem. Res.* **2004**, *37*, 580−591. (d) List, B. *Acc. Chem. Res.* **2004**, *37*, 548−557. (e) Bock, D. A.; Lehmann, C. W.; List, B. *Proc. Natl. Acad. Sci. U.S.A.* **2010**, *107*, 20636−20641.

(2) Allemann, C.; Gordillo, R.; Clemente, F. R.; Cheong, P. H.-Y.; Houk, K. N. *Acc. Chem. Res.* **2004**, *37*, 558−569.

(3) (a) Eder, U.; Sauer, G.; Wiechert, R. *Angew. Chem., Int. Ed.* **1971**, *10*, 496−497. (b) Hajos, Z. G.; Parrish, D. R. *J. Org. Chem.* **1974**, *39*, 1615−1621. (c) Cohen, N. *Acc. Chem. Res.* **1976**, *9*, 412−417.

(4) Bisai, V.; Bisai, A.; Singh, V. K. *Tetrahedron* **2012**, *68*, 4541−4580.

(5) (a) Barbas, C. F., III *Angew. Chem., Int. Ed.* **2008**, *47*, 42−47. (b) Melchiorre, P.; Marigo, M.; Carlone, A.; Bartoli, G. *Angew. Chem., Int. Ed.* **2008**, *47*, 6138−6171.

(6) (a) Dondoni, A.; Massi, A. *Angew. Chem., Int. Ed.* **2008**, *47*, 4638−4660. (b) MacMillan, D. W. C. *Nature* **2008**, *455*, 304−308. (c) Zhao, J. H. L.; Jiang, J.; Tang, Z.; Cun, L.; Gong, L. *Tetrahedron Lett.* **2008**, *49*, 3372−3375. (d) Mukherjee, S.; Yang, J. W.; Hoffmann, S.; List, B. *Chem. Rev.* **2007**, *107*, 5471−5569. (e) Raj, M.; Vishnumaya; Ginotra, S. K.; Singh, V. K. *Org. Lett.* **2006**, *8*, 4097−4099. (f) Dziedzic, P. Z. W.; Hafren, J.; Cordova, A. *Org. Biomol. Chem.* **2006**, *4*, 38−40. (g) Tang, Z.; Yang, Z.-H.; Chen, X.-H.; Cun, L.-F.; Mi, A.-Q.; Jiang, Y.-Z.; Gong, L.-Z. *J. Am. Chem. Soc.* **2005**, *127*, 9285−9289. (h) Tang, Z.; Jiang, F.; Cui, X.; Gong, L.; Mi, A.; Jiang, Y.; Wu, Y. *Proc. Natl. Acad. Sci. U.S.A.* **2004**, *101*, 5755−5760. (i) Machajewski, T. D.; Wong, C. *Angew. Chem., Int. Ed.* **2000**, *39*, 1352−1374.

(7) Vishnumaya, M. R.; Singh, V. K. *J. Org. Chem.* **2009**, *74*, 4289−4297.

(8) Maya, V.; Raj, M.; Singh, V. K. *Org. Lett.* **2007**, *9*, 2593−2595.

(9) Tang, Z.; Jiang, F.; Yu, L.-T.; Cui, X.; Gong, L.-Z.; Mi, A.-Q.; Jiang, Y.-Z.; Wu, Y.-D. *J. Am. Chem. Soc.* **2003**, *125*, 5262−5263.

(10) (a) Ribas-Arino, J.; Carvajal, M. A.; Chaumont, A.; Masia, M. *Chem.—Eur. J.* **2012**, *18*, 15868−15874. (b) Tang, G.; Hu, X.; Altenbach, H. J. *Tetrahedron Lett.* **2011**, *52*, 7034−7037. (c) Bhowmick, S.; Bhowmick, K. C. *Tetrahedron Asymmetry* **2011**, *22*, 1945−1979. (d) Aratake, S.; Itoh, T.; Okano, T.; Usui, T.; Shoji, M.; Hayashi, Y. *Chem. Commun.* **2007**, 2524−2526. (e) Guizzetti, S.; Benaglia, M.; Raimondi, L.; Celentano, G. *Org. Lett.* **2007**, *9*, 1247−1250.

(11) Mase, N.; Nakai, Y.; Ohara, N.; Yoda, H.; Takabe, K.; Tanaka, F.; Barbas, C. F., III *J. Am. Chem. Soc.* **2006**, *128*, 734−735.

(12) (a) Hayashi, Y.; Sumiya, T.; Takahashi, J.; Gotoh, H.; Urushima, T.; Shoji, M. *Angew. Chem., Int. Ed.* **2006**, *45*, 958−961. (b) Hayashi, Y.; Aratake, S.; Okano, T.; Takahashi, J.; Sumiya, T.; Shoji, M. *Angew. Chem., Int. Ed.* **2006**, *45*, 5527−5529.

(13) (a) Narayan, S.; Muldoon, J.; Finn, M. G.; Fokin, V. V.; Kolb, H. C.; Sharpless, K. B. *Angew. Chem., Int. Ed.* **2005**, *44*, 3275−3279. (b) Narayan, S.; Fokin, V. V.; Sharpless, K. B. In *Organic Reactions in Water*; Blackwell Publishing Ltd.: Oxford, UK, 2007; pp 350−365.

(14) (a) Hayashi, Y. *Angew. Chem., Int. Ed.* **2006**, *45*, 8103−8104. (b) Klijn, J. E.; Engberts, J. B. F. N. *Nature* **2005**, *435*, 746−747.

(15) Wagner, J.; Lerner, R. A.; Barbas, C. F., III *Science* **1995**, *270*, 1797−1800.
(16) Barbas, C. F., III; Heine, A.; Zhong, G.; Hoffmann, T.; Gramatikova, S.; Björnestedt, R.; List, B.; Anderson, J.; Stura, E. A.; Wilson, I. A.; Lerner, R. A. *Science* **1997**, *278*, 2085−2092.
(17) Zhong, G.; Hoffmann, T.; Lerner, R. A.; Danishefsky, S.; Barbas, C. F., III *J. Am. Chem. Soc.* **1997**, *119*, 8131−8132.
(18) Hoffmann, T.; Zhong, G.; List, B.; Shabat, D.; Anderson, J.; Gramatikova, S.; Lerner, R. A.; Barbas, C. F., III *J. Am. Chem. Soc.* **1998**, *120*, 2768−2779.
(19) Bertelsen, S.; Jørgensen, K. A. *Chem. Soc. Rev.* **2009**, *38*, 2178−2189.
(20) Zhu, X.; Tanaka, F.; Lerner, R. A.; Barbas, C. F., III; Wilson, I. A. *J. Am. Chem. Soc.* **2009**, *131*, 18206−18207.
(21) Bahmanyar, S.; Houk, K. N. *J. Am. Chem. Soc.* **2001**, *123*, 11273−11283.
(22) Bahmanyar, S.; Houk, K. N.; Martin, H. J.; List, B. *J. Am. Chem. Soc.* **2003**, *125*, 2475−2479.
(23) (a) Clemente, F. R.; Houk, K. N. *Angew. Chem., Int. Ed.* **2004**, *43*, 5766−5768. (b) Clemente, F. R.; Houk, K. N. *J. Am. Chem. Soc.* **2005**, *127*, 11294−11302. (c) Zhang, X.; Houk, K. N. *J. Org. Chem.* **2005**, *70*, 9712−9716. (d) Zhao, Q.; Lam, Y.-h.; Kheirabadi, M.; Xu, C.; Houk, K. N.; Schafmeister, C. E. *J. Org. Chem.* **2012**, *77*, 4784−4792. (e) Cheong, P. H.-Y.; Legault, C. Y.; Um, J. M.; Çelebi-Ölçüm, N.; Houk, K. N. *Chem. Rev.* **2011**, *111*, 5042−5137.
(24) Zhu, H.; Clemente, F. R.; Houk, K. N.; Meyer, M. P. *J. Am. Chem. Soc.* **2009**, *131*, 1632−1633.
(25) Allemann, C.; Uma, J. M.; Houk, K. N. *J. Mol. Catal. A: Chem.* **2010**, *324*, 31−38.
(26) Zhu, X.; Tanaka, F.; Hu, Y.; Heine, A.; Fuller, R.; Zhong, G.; Olson, A. J.; Lerner, R. A.; Barbas, C. F., III; Wilson, I. A. *J. Mol. Biol.* **2004**, *343*, 1269−1280.
(27) Jorgensen, W. L.; Tirado-Rives, J. *J. Comput. Chem.* **2005**, *26*, 1689−1700.
(28) Acevedo, O.; Jorgensen, W. L. *Acc. Chem. Res.* **2010**, *43*, 142−151.
(29) Allen, C.; Sambasivarao, S. V.; Acevedo, O. *J. Am. Chem. Soc.* **2013**, *135*, 1065−1072.
(30) Acevedo, O.; Armacost, K. *J. Am. Chem. Soc.* **2010**, *132*, 1966−1975.
(31) Sheppard, A. N.; Acevedo, O. *J. Am. Chem. Soc.* **2009**, *131*, 2530−2540.
(32) Acevedo, O. *J. Phys. Chem. B* **2009**, *113*, 15372−15381.
(33) Jorgensen, W. L.; Chandrasekhar, J.; Madura, J. D.; Impey, W.; Klein, M. L. *J. Chem. Phys.* **1983**, *79*, 926−935.
(34) Kurtz, S. S., Jr.; Wikingsson, A. E.; Camin, D. L.; Thompson, A. R. *J. Chem. Eng. Data* **1965**, *10*, 330−334.
(35) Chickos, J. S.; Acree, W. E. *J. Phys. Chem. Ref. Data* **2003**, *32*, 519−878.
(36) Thompson, J. D.; Cramer, C. J.; Truhlar, D. G. *J. Comput. Chem.* **2003**, *24*, 1291−1304.
(37) Vilseck, J. Z.; Sambasivarao, S. V.; Acevedo, O. *J. Comput. Chem.* **2011**, *32*, 2836−2842.
(38) Kaminski, G. A.; Friesner, R. A.; Tirado-Rives, J.; Jorgensen, W. L. *J. Phys. Chem. B* **2001**, *105*, 6474−6487.
(39) Tubert-Brohman, I.; Acevedo, O.; Jorgensen, W. L. *J. Am. Chem. Soc.* **2006**, *128*, 16904−16913.
(40) Sambasivarao, S. V.; Acevedo, O. *J. Chem. Theory Comput.* **2009**, *5*, 1038−1050.
(41) Reymond, J.-L. *J. Mol. Catal. B: Enzym.* **1998**, *5*, 331−337.
(42) (a) Zhong, G.; Shabat, D.; List, B.; Anderson, J.; Sinha, S. C.; Lerner, R. A.; Barbas, C. F., III *Angew. Chem., Int. Ed.* **1998**, *37*, 2481−2484. (b) Zhong, G.; Lerner, R. A.; Barbas, C. F., III *Angew. Chem., Int. Ed.* **1999**, *38*, 3738−3741. (c) Turner, J. M.; Bui, T.; Lerner, R. A.; Barbas, C. F., III; List, B. *Chem.—Eur. J.* **2000**, *6*, 2772−2774. (d) Tanaka, F.; Barbas, C. F., III *J. Immunol. Methods* **2002**, *269*, 67−79. (e) Karlstrom, A.; Zhong, G.; Rader, C.; Larsen, N. A.; Heine, A.; Fuller, R.; List, B.; Tanaka, F.; Wilson, I. A.; Barbas, C. F., III; Lerner, R. A. *Proc. Natl. Acad. Sci. U.S.A.* **2000**, *97*, 3878−3883.
(43) Arnó, M.; Domingo, L. R. *Org. Biomol. Chem.* **2003**, *1*, 637−643.
(44) (a) Alexandrova, A. N.; Röthlisberger, D.; Baker, D.; Jorgensen, W. L. *J. Am. Chem. Soc.* **2008**, *103*, 15907−15915. (b) Röthlisberger, D.; Khersonsky, O.; Wollacott, A. M.; Jiang, L.; DeChancie, J.; Betker, J.; Gallaher, J. L.; Althoff, E. A.; Zanghellini, A.; Dym, O.; Albeck, S.; Houk, K. N.; Tawfik, D. S.; Baker, D. *Nature* **2008**, *453*, 190−195.
(45) Jiang, L.; Althoff, E. A.; Clemente, F. R.; Doyle, L.; Röthlisberger, D.; Zanghellini, A.; Gallaher, J. L.; Betker, J. L.; Tanaka, F.; Barbas, C. F., III; Hilvert, D.; Houk, K. N.; Stoddard, B. L.; Baker, D. *Science* **2008**, *319*, 1387−1391.
(46) Frisch, M. J.et al., revision B.01; Gaussian, Inc.: Wallingford, CT, 2009; full reference given in SI.
(47) Schmid, M. B.; Zeitler, K.; Gschwind, R. M. *Chem. Sci.* **2011**, *2*, 1793−1803.
(48) DeChancie, J.; Acevedo, O.; Evanseck, J. D. *J. Am. Chem. Soc.* **2004**, *126*, 6043−6047.